International Journal of Concrete Structures and Materials

RESEARCH Open Access

Physicochemical Properties of Cementitious Materials with Spent Coffee Ground Ash

Yoonsuk Choi[1] and Byoungsun Park[2*]

Abstract

With the increasing global consumption of coffee, a substantial amount of spent coffee grounds (SCG) is generated. To address this, research has focused on recycling SCG as a renewable fuel, including the production of SCG pellets. When used as fuel in biomass-fired power plants, SCG pellets generate SCG ash, which necessitates effective utilization strategies. This study evaluates the potential of SCG ash as a supplementary cementitious material (SCM) by investigating its effects on concrete properties. SCG ash was produced by drying SCG at 110 °C and combusting it at 900 °C. Concrete specimens were prepared by replacing ordinary Portland cement (OPC) with SCG ash at 5%, 10%, and 15% substitution levels. Fly ash (FA) and blast furnace slag (BFS) were also incorporated to analyze hydration kinetics. X-ray diffraction (XRD) and thermogravimetric analyses confirmed the presence of calcite in SCG ash specimens, while mercury intrusion porosimetry indicated increased porosity with higher SCG ash content. Isothermal calorimetry revealed reduced hydration heat with increasing SCG ash replacement. Notably, concrete containing 5% SCG ash exhibited mechanical properties and durability comparable to plain concrete. Based on these findings, 5% was determined to be the optimal SCG ash substitution level. This study suggests that incorporating SCG ash into concrete can reduce CO_2 emissions from cement production while providing a sustainable recycling method for SCG ash.

Keywords Spent coffee ground ash, Supplementary cementitious materials, Hydrates analysis, Compressive strength, Microstructure

1 Introduction

Coffee is one of the most preferred beverages worldwide. In South Korea, it is the second most traded commodity after oil (Murty et al., 2012). According to the International Coffee Organization, annual coffee production has increased from 140 million packets to 152 million packets since 2010. By 2021, approximately 166.63 million packets (60 kg per bag) of coffee were consumed globally, compared to 164 million packets (60 kg per bag) in 2019 (Statista.com, 2022). n average, only 10% of coffee beans are used to make coffee beverages, while the remaining 90% of spent coffee grounds (SCG) are disposed of in landfills (Blinová et al., 2017). SCG contain compounds such as caffeine, tannins, and polyphenols, which are harmful to the environment. The decomposition of this organic matter in landfills requires large amounts of oxygen (Janissen et al., 2018; Kim et al., 2020). Consequently, various studies have been conducted to address the environmental issues associated with SCG. SCG are organic waste with a high nitrogen content and are primarily used for composting as plant fertilizers (Santos et al., 2017; Liu et al., 2011) or as soil amendments (Cervera-Mata et al., 2020, 2021). However, they also contain the phytotoxic compound chlorogenic acid, which limits their use (Franklin et al., 2011). Several studies are investigating the production of carbonaceous adsorbents from SCG for water treatment purposes (Namane et al., 2005;

*Correspondence:
Byoungsun Park
bspark0927@korea.ac.kr
[1] Smart Construction Materials Center, Korea Conformity Laboratories, Cheongju-Si, Chungbuk 28115, Republic of Korea
[2] Department of Environmental Systems Engineering, Sejong Campus, Korea University, Sejong-Si 30019, Republic of Korea

Pagalan et al., 2020). Due to resource depletion, environmental concerns, and unstable oil prices, extensive research is being conducted on the development of alternative fuels using biomass resources. The lower heating value of dry SCG is higher than that of other solid biomass resources (Kang et al., 2017). Consequently, studies are exploring renewable fuels, such as pellet manufacturing and oil extraction, utilizing coffee by-products like coffee husks and SCG (Colantoni et al., 2021; Lee et al., 2022; Limousy et al., 2013; Najdanovic-Visak et al., 2017; Park et al., 2020; Setter et al., 2020). Following the burning of SCG, SCG ash remains. Given the substantial amount of SCG generated, technologies for processing SCG ash are needed. However, research on SCG ash recycling remains insufficient.

The traditional construction industry raises significant concerns regarding its carbon footprint and environmental impact due to high carbon dioxide emissions and waste generation (Saberian et al., 2021). Consequently, in civil engineering, applied research is being conducted to utilize industrial by-products that occur in large quantities, such as SCG. Previous studies have explored mixing SCG with binders and other industrial by-products for use in construction materials, including road subgrade materials, embankment fill materials, and non-structural construction materials. Arulrahah et al. applied SCG mixed with fly ash (FA) to evaluate its potential use as a road embankment non-structural fill material (Arulrajah et al., 2014, 2016, 2017a, 2017b). Kua et al. proposed a mixture of SCG, blast furnace slag (BFS), and FA to meet the structural strength requirements of road subgrade materials (Kua et al., 2016). They also examined the leaching of contaminants from this byproduct-based material and reviewed the stiffness and deformation characteristics of SCG-based geopolymer (Kua et al., 2017, 2019). Le et al. investigated the strength characteristics of specimens in which SCG and oyster shells were mixed with an alkali-activated material based on BFS (Le et al., 2021). Suksiripattanapong et al. mixed SCG and rice husk ash with BFS based geopolymer and evaluated their strength and microstructure to develop construction subgrade materials (Suksiripattanapong et al., 2017). Most studies on the use of SCG as construction material involve mixing it with industrial by-products such as FA and BFS to produce geopolymer composites. These composites, primarily intended for road subgrade applications, offer a way to recycle large quantities of SCG without requiring complex pretreatment processes. However, SCG is currently limited to non-structural applications, and research on its potential use in cementitious materials remains insufficient.

SCG contains significant amounts of organic matter, including fatty acids, cellulose, hemicellulose, and polysaccharides like lignin, making it difficult to incorporate into cement-based materials (Campos-Vega et al., 2015). Therefore, to use SCG as a supplementary cementitious material, it must be chemically stabilized, and any negative effects on engineering properties must be mitigated. SCG ash, a by-product generated when SCG is used as fuel, is largely free of organic matter. Consequently, concrete produced using SCG ash has the potential for structural applications.

Several researchers have conducted pyrolysis processes to recycle SCG as a concrete component. Roychand et al. pyrolyzed SCG at 350 °C and 500 °C and fabricated concrete by replacing 5%, 10%, 15%, and 20% of fine aggregates with the pyrolyzed SCG (Roychand et al., 2023). They reported a 29.3% increase in compressive strength when fine aggregates were replaced with SCG pyrolyzed at 350 °C. They also conducted a field study by applying concrete incorporating the developed coffee biochar at an actual construction site (Roychand et al., 2025). This study examined the slump, compressive strength, and shrinkage characteristics of the concrete. The results indicated an increase in the slump of the coffee biochar-modified concrete. Additionally, while the compressive strength decreased at early ages, it showed an increase at 54 days. Furthermore, a reduction in shrinkage was also reported. Jie Shao et al. investigated the properties of concrete using SCG hydrothermal biochar, prepared through a low-temperature hydrothermal process, as a fine aggregate (Shao et al., 2024). They found that SCG hydrothermal biochar reduced the concrete slump and that the mechanical performance varied depending on the amount of biochar added. Laboratory studies have confirmed that SCG can be used as a concrete component through pyrolysis. However, the pyrolysis process is expensive and generates CO_2 due to the high temperatures required. Therefore, a recycling technology that does not produce additional CO_2 emissions during processing is needed. One alternative method for recycling SCG is the manufacture of bio-pellets, which can be used in thermal power plants. This process generates SCG ash as a byproduct, necessitating the development of technologies to process this ash. However, there have been few studies on using SCG ash as a concrete component. Thus, further research is needed to determine whether SCG ash can be effectively utilized in concrete.

In this study, the physicochemical properties of cementitious materials containing SCG ash were investigated. SCG was incinerated at 900 °C and pulverized to obtain SCG ash. In fabricating the cementitious materials, ordinary Portland cement (OPC) was partially replaced with 5%, 10%, and 15% SCG ash. To examine the effect

of SCG ash on the hydration properties of cementitious materials, hydrates and microstructures were evaluated using cement paste specimens. Additionally, the effects of SCG ash on the mechanical properties and durability of cementitious materials were assessed using concrete specimens.

2 Materials and Methods

This section outlines the experimental procedures used to investigate the physicochemical, mechanical, durability, shrinkage, and microstructural properties of concrete incorporating SCG ash. Figure 1 illustrates the research methodology adopted in this study.

2.1 Materials

Initially, the spent coffee grounds (SCG) were dried at 100 ± 5 °C for 24 h in a drying furnace to remove moisture. SCG ash was then produced through a high-temperature incineration process in a sintering furnace at 900 °C or higher to eliminate organic matter, as shown in Fig. 2. When SCG was exposed to temperatures of 900 °C or higher, the organic compounds underwent thermal decomposition and combustion. SCG contains various organic substances, including fatty acids, cellulose, hemicellulose, lignin, and other polysaccharides, which gradually decompose at elevated temperatures (Acchar & Dultra, 2013). The dehydrated SCG was incinerated in a sintering furnace at approximately 900 °C for 2 h, then cooled for 10 h with the furnace open. The resulting SCG ash was processed into SCG ash powder with a Blaine fineness of 4170 cm^2/g and a specific gravity of 1.98 g/cm^3 using a ball mill.

In this study, Type I OPC, specified in ASTM C150-21 (ASTM C150/C150M-21, 2021), was used as the binder for concrete, while FA and BFS were used as supplementary cementitious materials. Table 1 presents the physical properties and chemical composition of the binder, including SCG ash. The FA was classified as Class F, with $SiO_2 + Al_2O_3 + Fe_2O_3$ content of 70% or more and a loss on ignition (LOI) of 6% or less. Notably, SCG ash exhibited a lower specific gravity than the other materials. Specifically, its specific gravity was only 62% of that of OPC, leading to a higher binder-to-aggregate ratio in specimens containing SCG ash. SCG ash exhibited LOI due to the significant presence of organic compounds. Inorganic compounds, primarily potassium, followed by silicon, accounted for only 14% of the ash. Table 2 outlines the physical properties of the aggregates, with river sand used as the fine aggregate and crushed stone (G_{max} = 19 mm) as the coarse aggregate.

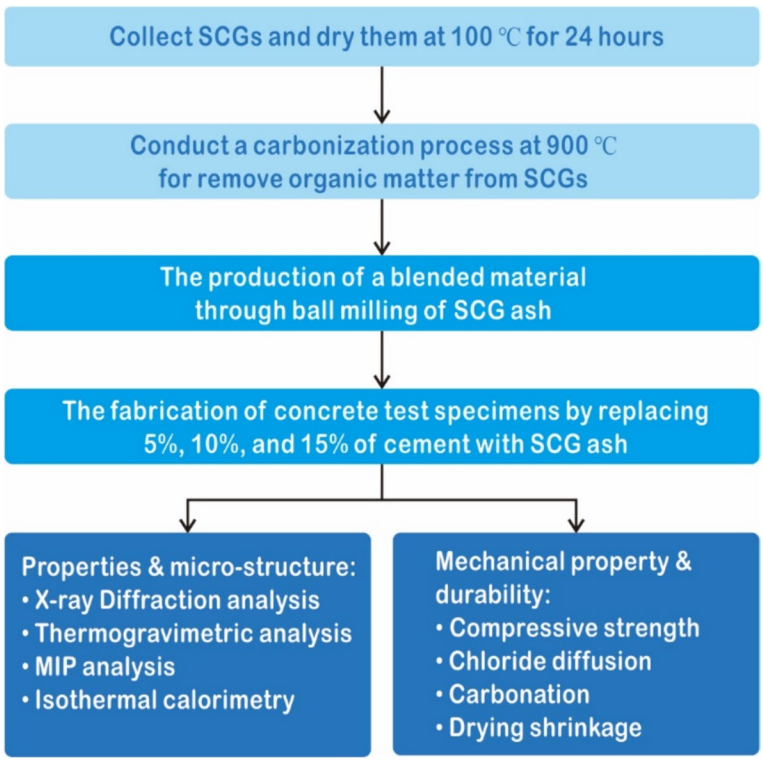

Fig. 1 Flowchart of experimental works

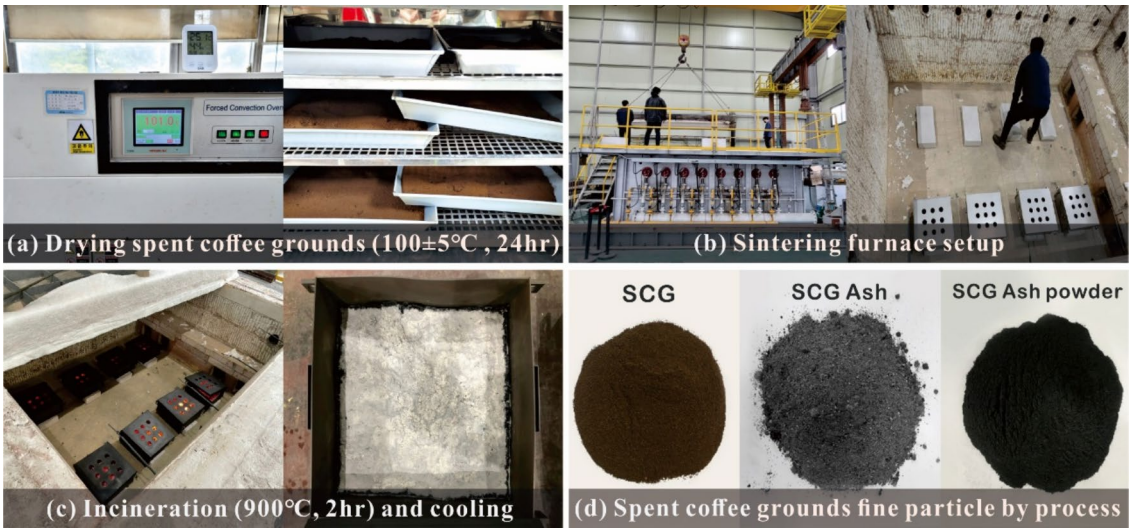

Fig. 2 SCG ash manufacturing process

Table 1 Physical and chemical composition of raw materials

Content		Materials			
		OPC	FA	BFS	SCG ash
Physical	Specific gravity	3.18	2.34	2.94	1.98
	Blaine (cm^2/g)	3760	4150	4750	4170
Chemical (wt, %)	SiO_2	19.86	57.96	34.13	0.07
	Al_2O_3	5.16	21.99	13.74	0.03
	TiO_2	0.28	1.02	0.56	N.D
	Fe_2O_3	3.25	6.10	0.47	0.05
	MgO	2.32	1.59	3.31	2.54
	CaO	62.02	4.57	45.01	1.11
	Na_2O	0.20	0.68	0.21	0.08
	K_2O	0.97	1.45	0.48	6.85
	MnO	0.31	0.10	0.15	0.02
	P_2O_5	0.18	0.54	0.03	2.36
	SO_3	2.45	0.33	1.91	0.66
	LOI	2.99	3.65	0.03	86.20

* *LOI* loss of ignition

Table 2 Physical properties of fine and coarse aggregates

Type	Density (g/cm^3)	Absorption (%)	Fineness modulus
Fine aggregate	2.62	1.30	3.10
Coarse aggregate	2.63	1.40	6.70

2.2 Mixture Proportions

Table 3 presents the mixture proportions of concrete, designed as a weight mixture while considering the specific gravity and density of each raw material. The water–binder ratio was maintained at 0.45. Concrete specimens were prepared by substituting OPC with 5%, 10%, and 15% SCG ash.20% FA and 30% BFS were also used as substitutes for OPC. The concrete specimens were manufactured following ASTM C192/C192M-19 guidelines, with the sizes of the concrete test specimens adjusted to meet the requirements of each test standard (ASTM C192/C192M-19, 2019). Three test specimens were produced for each variable. To evaluate the effect of SCG ash, concrete curing was conducted in a constant temperature and humidity room under environmental conditions of 20 °C and 60% relative humidity.

2.3 Test Methods

XRD and thermogravimetric analyses were performed to analyze the mineral compositions of the hydrates. Cement paste specimens were fabricated according to the specimen IDs in Table 3 to investigate the mineral composition of the hydrates. For example, "Plain" consisted of 100% OPC, while "FA20" consisted of 80% OPC and 20% FA by weight. The water-to-binder ratio of the specimens was fixed at 0.5. Mineral compositions of the hydrates were investigated using specimens at 91 days. After curing the cement paste for 91 days, hydration was stopped by substituting isopropyl alcohol and ethyl ether, respectively, and an analysis sample was prepared by evaporating the remaining ethyl ether using a dryer set to 40 °C. XRD analysis was conducted between 5° and 60° in the 2θ range, with a step size of 0.04° and a counting time of 2 s per step, using the S product of company R equipped with Cu-Kα radiation (λ = 1.5418 Å). Thermogravimetric analysis was performed using a thermogravimetry/

Table 3 Mixture proportion of concrete

No	Specimen ID	Unit weight (kg/m^3)						
		Water	OPC	Fine aggregate	Coarse aggregate	FA	BFS	SCGAsh
1	Plain	173	383	775	950	-	-	-
2	SCGAsh5	173	364	763	936	-	-	19
3	SCGAsh10	173	345	752	923	-	-	38
4	SCGAsh15	173	326	741	909	-	-	58
5	FA20	173	307	736	903	77	-	-
6	BFS30	173	268	729	894	-	115	-
7	FA20SCGAsh10	173	268	713	875	77		38
8	BFS30SCGAsh10	173	230	706	866	-	115	38

derivative thermogravimetry (TG-DTG) analyzer (SDT Q600, TA Instruments, USA). The TG-DTG analysis was carried out during heating at a rate of 10 °C /min in a nitrogen atmosphere (300 mL/min). The measured temperature ranged from 20 to 1000 °C.

The pore size distribution was determined according to the Mercury Intrusion Porosimeter of ASTM D 4284 and measured using an AutoPore IV9500 under the conditions of a contact angle of 130°, mercury surface tension of 485 dynes/cm, and mercury filling pressure of 0.53 psi (ASTM D4284-12, 2012). The paste specimens (same as specimens for XRD analysis) prepared for MIP measurement were measured after curing for 91 days and crushed to a size of 1–2 mm; the crushed samples were collected from the middle of the specimens to prevent sample unevenness. The crushed sample was vacuum-dried to halt hydration and prevent carbonation. To eliminate the effect of moisture, the samples were dried at approximately 50 °C for 24 h before measurement.

To investigate the effect of SCG ash on the hydration kinetics of cementitious materials, hydration heat was measured using isothermal calorimetry (TAM-AIR). The initial temperature was set to 23 °C as the standard temperature, and the baseline was stabilized for 2 h with the reference sample before experimentation. The experiment was conducted once the baseline was stable. Cement paste was used to measure hydration heat according to the binder ratio listed in Table 3. For each binder ratio, 100 g of binder and 50 g of distilled water were mixed in a glass beaker using a glass rod. After thorough mixing, approximately 5 g of paste was added to the sample. The sample was then subjected to isothermal calorimetry, and hydration heat was measured for 168 h.

To assess the mechanical performance of concrete mixed with SCG ash, compressive strength was measured following ASTM C39/C39-21 (ASTM C39/C39M-21, 2021). Cylindrical specimens with a diameter of 100 mm and height of 200 mm were fabricated using the mixture proportions outlined in Table 3. Compressive strengths of three specimens were measured at 7, 28, and 91 days, and the average values were recorded as the results. A universal testing machine with a capacity of 1000 kN supplied the compressive load, and the loading rate was set to 4.7 kN/s.

The durability of concrete mixed with SCG ash was evaluated through chloride diffusion, carbonation, and drying shrinkage tests. A rapid chloride migration test (RCMT) was conducted to assess chloride penetration resistance with SCG ash substitution. The RCMT followed the NT Build 492 "Chloride Migration Coefficient from Non-Steady-State Migration Experiments" test method (NT BUILD 492, 1999). Concrete specimens with a diameter of 100 mm and a thickness of 50 mm were cured for 91 days and then cut into 50 ± 2 mm sections for testing. Each cut specimen was immersed in water for at least 24 h before the chloride penetration test to prevent instantaneous absorption based on the internal moisture state. A 0.3 N sodium hydroxide (NaOH) solution was added to the anode cell, 10% sodium chloride (NaCl) solution was added to the catholyte, and a voltage of 30 V was applied for 8 h. After completing the RCMT, the specimens were split, and the chloride penetration depth was measured using the silver nitrate (0.1 N $AgNO_3$) colorimetric method. The average penetration depth of each test specimen was used to determine the diffusion coefficient using Fick's second law. The chloride diffusion coefficient of the concrete specimens incorporating SCG ash as OPC substitute was calculated using the following equation:

$$\frac{C(x,t)}{C_0} = 1 - erf\left(\frac{x}{\sqrt{aDt}}\right), \tag{1}$$

where and are the chloride concentrations at depth $x(cm)$ at exposure time $t(years)$, and the surface concentration of chloride measured in the concrete sample

(% *mass*), respectively, where x is the depth below the exposed surface in (m), D is the chloride diffusion coefficient in (m^2/s), and t is the exposure time in (s).

The test specimens for carbonation resistance were shaped in a prismatic form with dimensions of 100 mm × 100 mm × 400 mm. The remaining surfaces, except for the penetration surface, were coated with epoxy to induce unidirectional penetration. All specimens were tested at 14, 28, and 91 days under a carbon dioxide concentration of (5 ± 0.25)% by placing them in a CO_2 chamber at a temperature of (20 ± 2) °C and a relative humidity of (90 ± 5)% after curing for 28 days. During each exposure period, the specimens were split, and a 1% phenolphthalein solution was sprayed to measure the carbon dioxide penetration depth. The carbonation rate coefficient was calculated based on the age and penetration depth.

To examine the drying shrinkage of concrete mixed with SCG ash, prismatic concrete specimens measuring 100 × 100 × 400 mm with embedded strain gauges were prepared for each mixing variable. These specimens were placed in a constant temperature and humidity room at 20 °C and a relative humidity of 60%. Drying shrinkage was evaluated by measuring at 60-min intervals for 91 days using a data logger (Company T, 30 channels) after 24 h of concrete placement.

3 Results and Discussion

3.1 XRD and TGA

Figure 3a displays the XRD patterns of Plain, SCGAsh05, SCGAsh10, and SCGAsh15. Mainly, peaks for portlandite and ettringite were observed in the Plain, indicating the presence of cement hydrate, C_3S, C_2S, C_4AF, and gypsum, which are the unreacted clinker phases. The XRD patterns of specimens containing SCG ash closely resembled those of the Plain. Notably, the intensity of the portlandite peak decreased with increasing SCG ash content. Additionally, calcite peaks were observed in specimens with SCG ash, unlike the Plain. The firing of SCG at 900 °C led to the presence of carbon due to carbonation, and the formation of calcite resulted from the reaction between calcium in OPC and carbon in SCG ash. The decrease in the portlandite peak is believed to be due to the organic matter present in the SCG ash, which attaches to the surface of the cement particles and hinders their hydration. As the SCG ash content increases, the portlandite peak gradually decreases because a greater number of cement particles remain un-hydrated. Additionally, the calcite peak appears in specimens containing SCG ash. Calcite, which dissolves during the cement hydration process, supplies Ca^{2+} ions and contributes to the formation of C-S–H (Péra et al., 1999). However, this reaction appears to have been inhibited by the organic matter in the SCG ash. It seems that the hydration of C_3S and C_2S was impeded by the organic matter in the SCG ash, resulting in insufficient C-S–H formation. This reduction in C-S–H content is expected to lead to a decrease in strength.

Figure 3b illustrates the XRD patterns of FA20, BFS30, FA20SCGAsh10, and BFS30SCGAsh10. Peaks corresponding to portlandite and ettringite were observed for FA20 and BFS20, along with peaks for unreacted clinkers C_3S, C_2S, and C_4AF. Notably, a quartz peak appeared in FA20, indicating the presence of unreacted FA particles. Conversely, the portlandite peak decreased for BFS30SCGAsh10 and FA20SCGAsh10. Furthermore, hydrotalcite was detected in FA20SCGAsh10. Particularly, the appearance of calcite was associated with the substitution of SCG ash. Therefore, it is anticipated that SCG subjected to the firing process at 900 °C underwent carbonization and reacted with cement to produce calcite.

Figure 4a presents the thermogravimetric analysis (TGA) results for Plain, SCGAsh5, SCGAsh10, and SCGAsh15. Plain exhibited weight loss due to the decomposition of C-S–H and ettringite below 200 °C, with additional weight loss observed between 400 and 500 °C attributed to portlandite decomposition. Slight weight loss between 600 and 800 °C was also noted due to calcite decomposition. Specimens containing SCG ash showed reduced weight loss below 200 °C compared to Plain, attributed to decreased C-S–H and ettringite. However, the influence of SCG ash content on the reduction in C-S–H and ettringite weight loss was not evident. Weight loss from $Ca(OH)_2$ decomposition decreased with increasing SCG ash content, while weight loss between 600 and 800 °C increased in SCG ash specimens, indicative of calcite decomposition. This aligns with the presence of calcite observed in XRD patterns of SCG ash specimens. Weight loss between 600 and 800 °C is shown owing to the decomposition of calcite. It was confirmed that specimens containing SCG ash contained calcite. This was also observed in the XRD patterns of the specimens with SCG ash. The specimens with SCG ash show weight loss upper 800 °C. The weight loss increased with increasing SCG ash content. Weight loss upper 800 °C was shown owing to the burnt of un-fired SCG particles in SCG ash. SCG ash was fired at 900 °C for 2 h in this study, resulting in incineration of SCG ash at temperatures exceeding 800 °C. The material that decomposes above 800 °C is presumed to be organic matter present in SCG ash. Analysis of the graph indicates that as the SCG ash content increases, the amount of organic matter also increases. Consequently, the weight loss due to the decomposition of organic matter increases, resulting in a reduction in the weight change associated with the

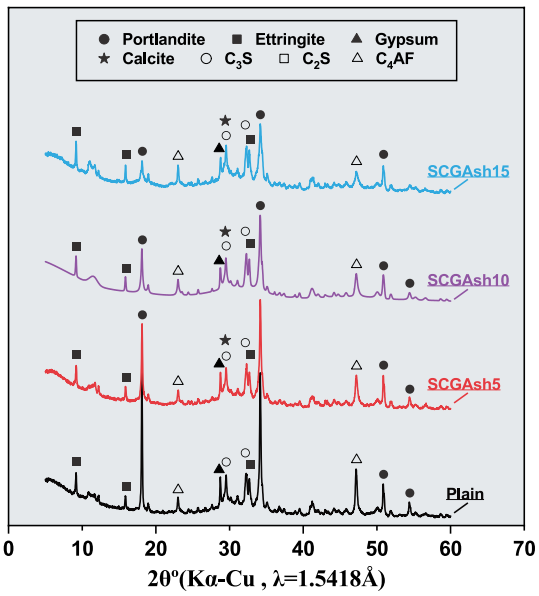

(a) XRD patterns of Plain, SCGAsh5, SCGAsh10, and SCGAsh15

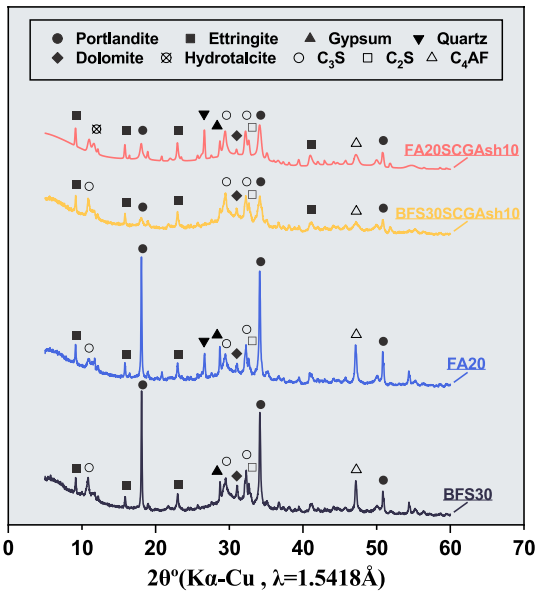

(b) XRD patterns of FA20SCGAsh10, BFS30SCGAsh10, FA20, and BFS30

Fig. 3 XRD patterns of specimens at 91 days

decomposition of C-S–H in the TGA analysis. Additionally, the XRD pattern analysis reveals a decrease in portlandite content. These findings suggest that the presence of unincinerated organic matter in SCG ash contributes to a reduction in concrete strength.

Figure 4b shows the TGA results for FA20, BFS30, FA20SCGAsh10, and BFS30SCGAsh10. FA20 and BFS30 exhibited weight losses below 200° C due to the decomposition of C-S–H and ettringite. The amount of weight loss of FA20 and BFS30 decreased compared to Plain,

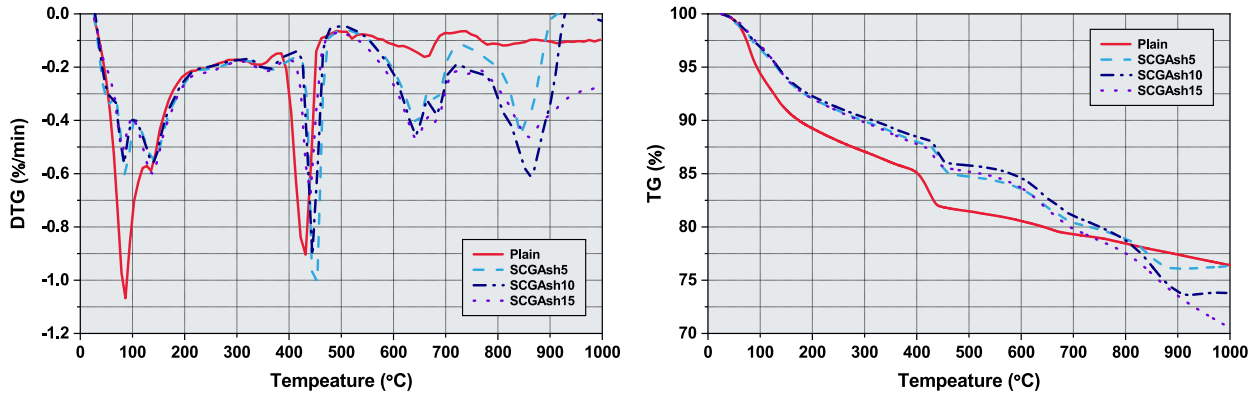

(a) Plain, SCGAsh5, SCGAsh10, and SCGAsh15

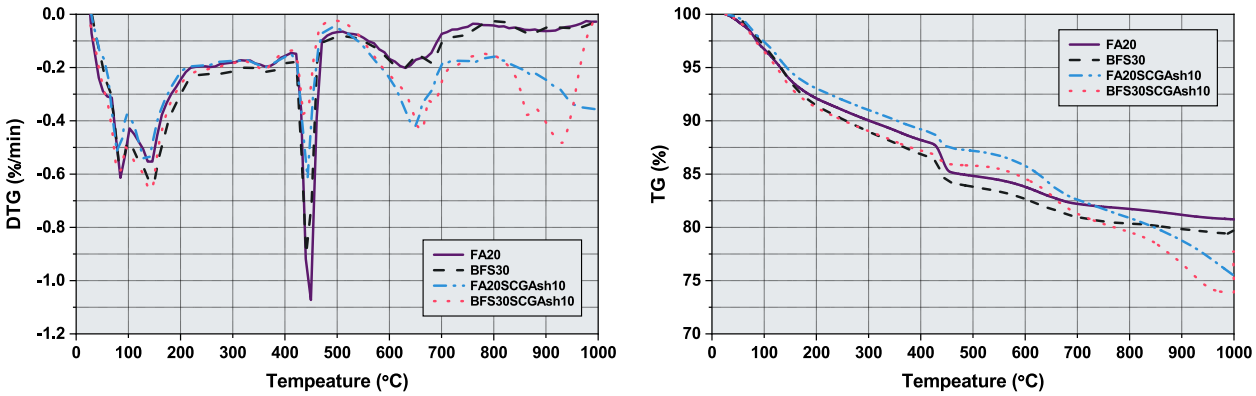

(b) FA20, BFS30, FA20SCGAsh10, and BFS30SCGAsh10

Fig. 4 Thermogravimetric analysis results

indicating a reduction in ettringite content due to FA and BFS substitution. Weight loss of FA20SCGAsh10 and BFS30SCGAsh10 was similar to that of FA20 and BFS30 below 200 °C, respectively, suggesting a minor effect of SCG ash substitution on weight loss in this temperature range. Weight loss between 400 and 500 °C was observed due to portlandite decomposition in FA20 and BFS30, with FA20 showing higher weight loss than BFS30, reflecting its higher portlandite content. The weight losses of FA20SCGAsh10 and BFS30SCGAsh10 were lower than FA20 and BFS30, indicating a reduction in portlandite content due to SCG ash, consistent with Fig. 4a. Weight loss between 600 and 800 °C was observed for FA20SCGAsh10 and BFS30SCGAsh10 due to calcite decomposition. Additionally, FA20SCGAsh10 and BFS30SCGAsh10 showed weight loss above 800 °C due to incineration of unburned organic matter in SCG ash.

3.2 Micropore Structure

Figure 5 illustrates the pore-size distribution graphs of the test specimens for each mixing variable. Examining the changes in the micropore structure due to the addition of SCG ash in Fig. 5a, pores with a size of 50 nm or more were predominantly distributed irrespective of the physical properties of the paste. Upon mixing SCG ash, the number of pores with a size of 100 nm or more increased. Additionally, the sample containing 5% SCG ash exhibited a micropore structure similar to that of OPC; however, with 10% or more SCG ash substitution,

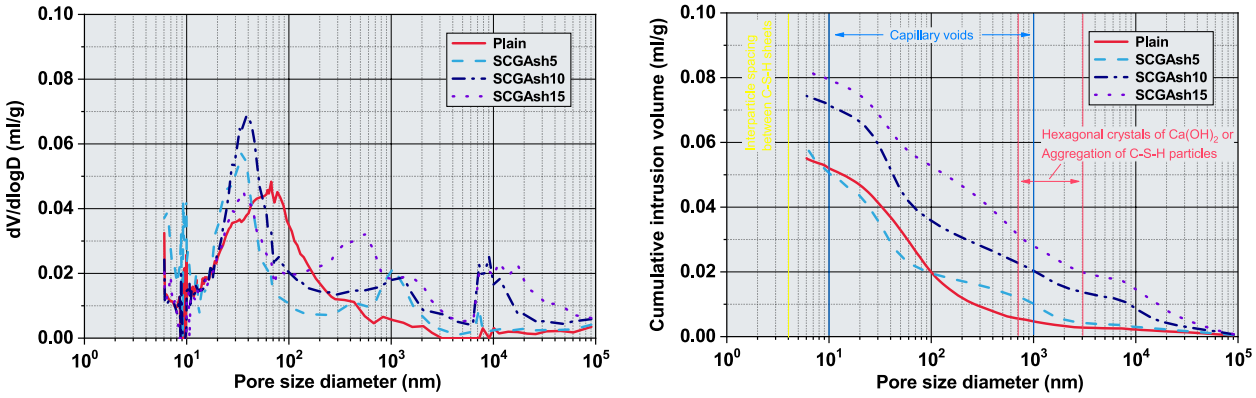

(a) Plain, SCGAsh5, SCGAsh10, and SCGAsh15

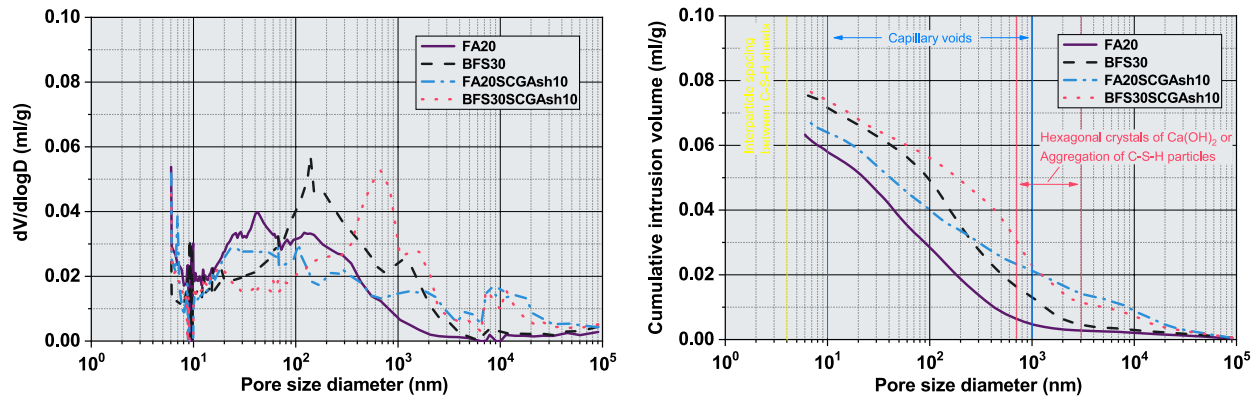

(b) FA20, BFS30, FA20SCGAsh10, and BFS30SCGAsh10

Fig. 5 Micropore structures analysis

the total number of voids increased. The graph shows a notable increase in pores at 10^4 nm. Capillary pores generated during the hydration process of cement typically measure 10^3 nm or less, and these pores are known to significantly influence the material's strength (Metha & Monteiro, 2014). Accordingly, it can be concluded that the 10^4 nm-sized pores are not a product of the cement hydration process. This observation can be attributed to the porous structure of SCG themselves, hindering pore densification through the hydration. An increase in pores with a size of 10^4 nm is expected to significantly reduce the mechanical performance of concrete.

In contrast, examining the micropore structure of the paste sample containing BFS and FA in Fig. 5b, the overall volume of voids decreased, and the internal pore structure was evenly distributed compared to OPC. This can be attributed to the latent hydraulic reaction of BFS and the pozzolanic reaction of FA, resulting in a dense internal void structure. Furthermore, substituting 10% of SCG ash resulted in a similar pore distribution, albeit with slightly larger overall void volume. As discussed earlier, this phenomenon occurs when porous SCG ash are substituted with cement, compared to cement and admixtures.

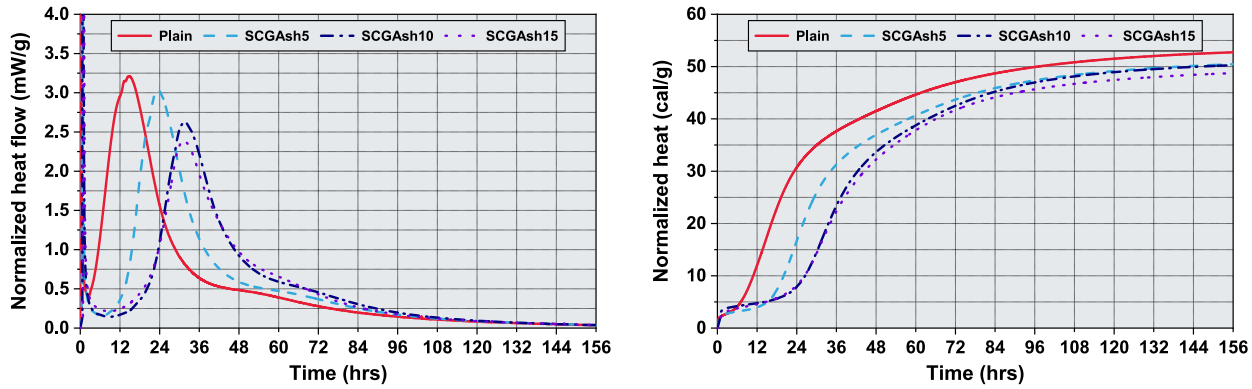

(a) Plain, SCGAsh5, SCGAsh10, and SCGAsh15

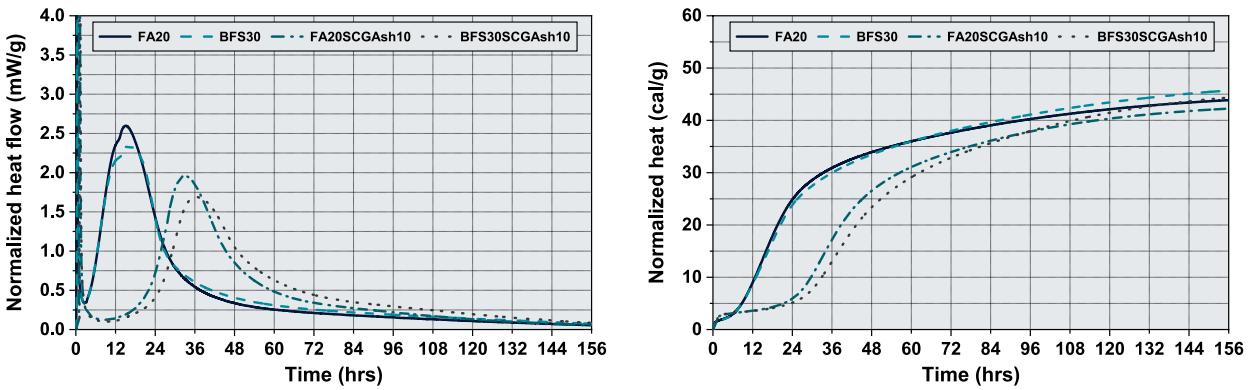

(b) FA20, BFS30, FA20SCGAsh10, and BFS30SCGAsh10

Fig. 6 Normalized heat flow and cumulative heat

3.2.1 Hydration Kinetics

Figure 6 presents the normalized heat flow and cumulative heat measured using isothermal calorimetry. In Fig. 6a, Plain exhibited the shortest induction period and highest peak during the acceleration period among the specimens. The induction period increased with SCG ash content, reaching 24 h when the SCG ash content exceeded 10%. The increase in the induction period is attributed to the organic matter in the SCG ash, which attaches to the cement particles and delays hydration. This delay is believed to have contributed to the decrease in the portlandite peak observed in XRD analysis and the reduction in C-S–H detected in TGA analysis. In specimens containing SCG ash, the induction period tended to increase; however, the shape of the graph after the induction period was similar to that of Plain. This suggests that SCG ash does not participate in the hydration reaction to form hydrates. Furthermore, XRD pattern did not reveal any hydrates other than calcite. Additionally, this delay in hydration is expected to hinder the normal hydration process, leading to an increase in porosity. In Fig. 5, it was observed that the porosity of the specimen containing SCG ash increased. Since SCG ash does not contribute to hydrate formation, an increase in its content may result in the generation of macropores at locations where SCG ash particles aggregate, potentially deteriorating the mechanical performance of concrete. Additionally, it is noted that the peak of the acceleration period decreased with increasing SCG ash content. The acceleration period initiates with the reaction of C_3S in the OPC (Makar et al., 2009). As the OPC content

decreased with increasing SCG ash content, so did the C_3S content, leading to a decrease in the acceleration period peak. Moreover, Plain showed the highest cumulative heat over the 168 h period. However, SCG ash led to a decrease in cumulative heat, although not proportionally to the SCG ash content.

As depicted in Fig. 6b, FA20 and BFS30 show lower peaks during the acceleration period, with FA20 exhibiting a higher peak intensity compared to BFS30. This discrepancy can be attributed to the fact that the pozzolanic reaction of FA and the latent hydraulic reaction of BFS commence after the formation of portlandite, resulting in a decrease in the acceleration peak proportional to the FA and BFS contents. However, the induction periods of FA20 and BFS30 resemble those of Plain. In contrast, the induction periods of FA20SCGAsh10 and BFS30SCGAsh10 are prolonged compared to FA20 and BFS30 due to SCG ash substitution, as evidenced in Fig. 6a. Given that the OPC content of FA20SCGAsh10 exceeds that of BFS30SCGAsh10, it is inferred that the acceleration period of FA20SCGAsh10 initiates faster than that of BFS30SCGAsh10. Furthermore, the cumulative heat of BFS30 surpasses that of FA20. This discrepancy arises from the fact that the heat generated by the pozzolanic reaction of FA is lesser than that generated by the latent hydraulic reaction of BFS (Qiang et al., 2016). Consequently, the cumulative heat of BFS30 appears larger than that of FA20. Despite the delayed initial strength development rate in specimens with SCG ash due to the extended induction period, the difference in cumulative heat after 168 h is minimal.

3.2.2 Compressive Strength

Figure 7 presents the compressive strength of each concrete mixture. In ordinary concrete, the compressive strength increases with the curing period. However, when FA and BFS admixtures are substituted, the strength does not increase compared to Plain, even with prolonged curing, due to the lack of potential hydraulic and pozzolanic reactions during water curing. Air-dry curing was conducted on all concrete test specimens to assess the effect of SCG ash.

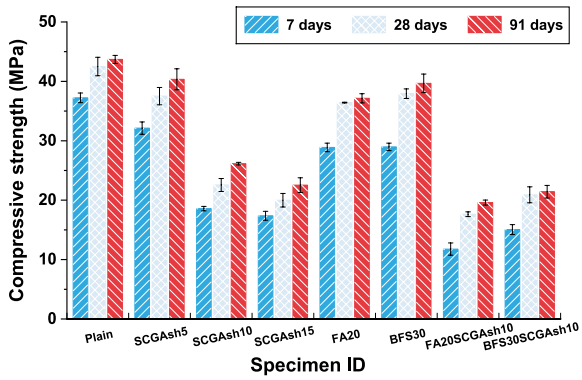

Fig. 7 Compressive strength

The compressive strength of plain concrete at 28 days was 42 MPa. When substituted with 5, 10, and 15% SCG ash, the compressive strengths were 38, 23, and 20 MPa, respectively. Compared to the reference 0.45OPC test specimen, the compressive strength decreased with increasing substitution rate of SCG ash by 5, 10, and 15%.

Particularly noteworthy is the rapid decrease in strength when 10% or more substitution occurs, consistent with the micropore structure and XRD results described earlier. As the main binder cement decreases and the amount of SCG ash increases, the hydration product decreases, and the internal structure density deteriorates, leading to decreased strength. Therefore, it is evident that the compressive strength of the specimens mixed with SCG ash and mineral admixture did not improve.

Finally, considering the stress–strain curve according to the substitution rate of SCG ash in Fig. 8, Plain displays a typical stress–strain curve shape of concrete, with the strain at the point of maximum stress between 0.002 and 0.003. In contrast, the SCGAsh5 test specimen, exhibits a maximum stress similar to that of Plain; however, the strain at the maximum stress is higher than that of the Plain. Furthermore, as the substitution rate of SCG ash increases to 10% or more, the maximum stress decreases rapidly, and the deformation rate increases, indicating a tendency for plastic failure.

3.3 Durability

Based on the RCMT results, Fig. 9 illustrates the chloride diffusion coefficients of the concrete test specimens in which the SCG ash were replaced with OPC. The results show that the chloride diffusion coefficient of the concrete mixed with SCG ash was higher than that of Plain, and the diffusion coefficient increased as the substitution amount increased. In other words, the micropore structure showed that the penetration resistance of chlorine ions decreased as the porous SCG ash was mixed. Nonetheless, SCGAsh5 had a higher diffusion coefficient than Plain but a lower diffusion coefficient than FA20.

Therefore, we can conclude that BFS30 had a lower chloride diffusion coefficient than Plain), which can be seen as an improved resistance to chloride permeation as the internal structure became denser owing to the reaction between the hydrate and BFS. Additionally, BFS30SCGAsh10 showed a lower chloride diffusion coefficient

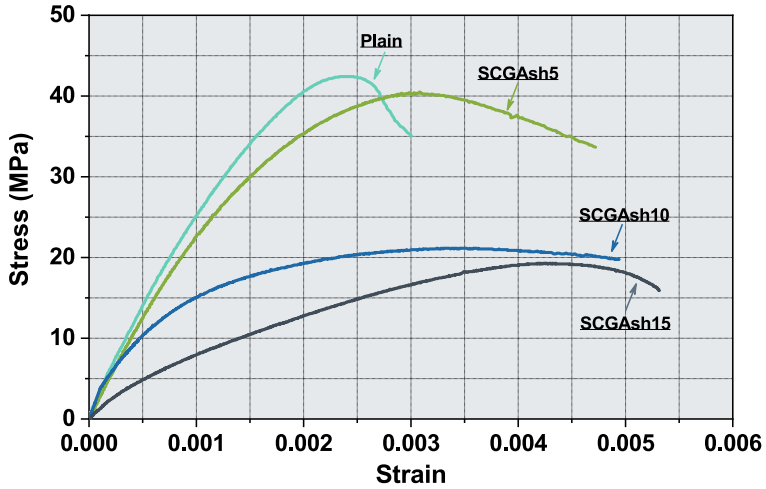

Fig. 8 Stress–strain curve at 91 days

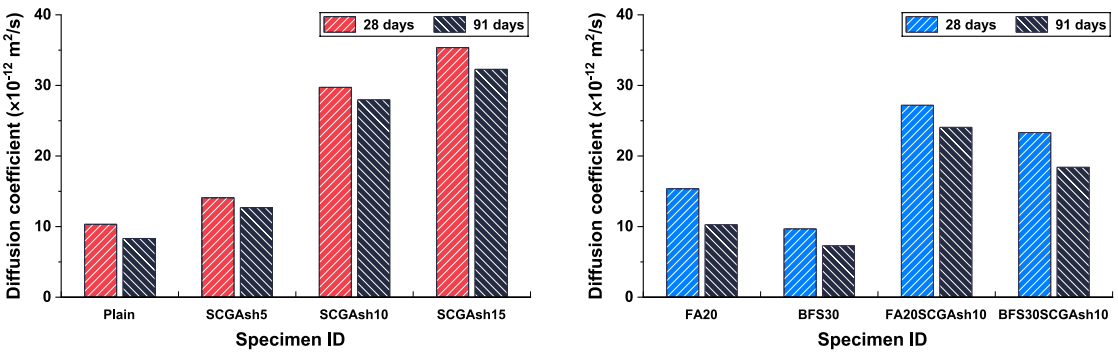

(a) Plain, SCGAsh5, SCGAsh10, and SCGAsh15 (b) FA20, BFS30, FA20SCGAsh10, and BFS30SCGAsh10

Fig. 9 Chloride diffusion coefficient determined by NT Build 492

than that of SCGAsh10, thereby indicating that BFS was effective.

Figure 10 illustrates the carbonation depth according to the exposure time to carbon dioxide of the specimens mixed with SCG ash. From the results, it is evident that the carbonation depth increased as the exposure time to CO_2 increased, regardless of the physical properties of the concrete, and the carbonation depth of the specimens mixed with the mineral admixture was small. Additionally, concrete mixed with SCG ash had a greater depth of carbonation than Plain, and the carbonation resistance decreased as the substitution rate increased. Similar to chloride diffusivity, the result of favoring durability did not appear, even when SCG ash and mineral admixture were used together.

Finally, Fig. 11 presents the results of measuring the change in drying shrinkage for each mixing variable of the concrete. The plain and FA20 specimens exhibited the lowest drying shrinkage, whereas BFS30 showed an increase in drying shrinkage. Conversely, specimens substituted with SCG ash showed an increase in drying shrinkage, where the higher the substitution rate of SCG ash, the greater was the drying shrinkage owing to the relatively high moisture absorption rate of the porous SCG ash; therefore, the drying shrinkage was significantly large. Because the drying shrinkage experiment in this study evaluated the drying shrinkage

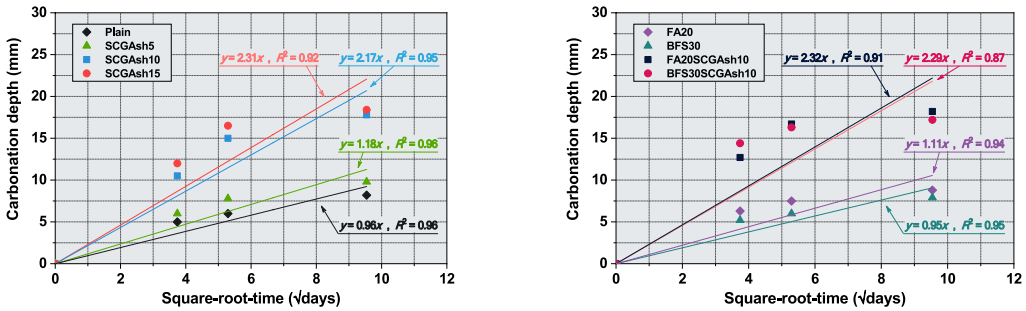

(a) Plain, SCGAsh5, SCGAsh10, and SCGAsh15 (b) FA20, BFS30, FA20SCGAsh10, and BFS30SCGAsh10

Fig. 10 Carbonation depth at 14 d, 28 d, 91 d

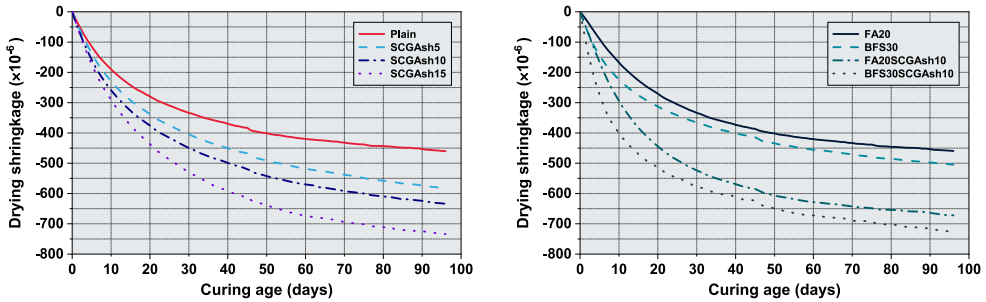

(a) Plain, SCGAsh5, SCGAsh10, and SCGAsh15 (b) FA20, BFS30, FA20SCGAsh10, BFS30 SCGAsh10

Fig. 11 Drying shrinkage

under air-dry curing conditions, there are some differences from concrete cured in water.

4 Conclusion

In this study, the physicochemical properties of cementitious materials were investigated by substituting OPC with SCG ash at varying percentages (5%, 10%, and 15% by weight). The SCG was subjected to high-temperature incineration to remove organic matter and then pulverized to prepare SCG ash. SCG ash was used to replace OPC at 5, 10, and 15% by weight. The hydration products were examined using X-ray diffraction and TGA analysis, and the hydration kinetics were investigated using isothermal calorimetry. The microstructures were investigated by MIP analysis. The compressive strengths of the concrete specimens were used to evaluate their mechanical properties. The chloride diffusivity, carbonation depth, and dry shrinkage of concrete specimens were measured to evaluate their durability. The following conclusions were drawn:

(1) Analysis of the cement hydrates revealed that no new hydrates were present in the specimens containing SCG ash. This finding suggests that SCG ash does not participate in the hydration process and functions primarily as a filler.
(2) It was confirmed that a large amount of organic matter existed in SCG ash even though it was incinerated at a temperature of 900 °C. The organic matter of SCG ash was found to interfere with the hydration of cement and increase macropores, thereby reducing the compressive strength and elastic modulus.
(3) The macropores generated by adding SCG ash were found to reduce the salt resistance and carbonation

resistance of concrete and significantly increase the drying shrinkage.

(4) Concrete with 5% cement substituted with SCG ash showed similar mechanical performance and durability to general OPC concrete. Therefore, the optimal substitution rate of SCG ash for use as a concrete admixture is 5%.

Acknowledgements
Not applicable.

Author contributions
Yoonsuk Choi: validation, formal analysis, investigation, writing—original draft, funding acquisition, methodology. Byoungsun Park: conceptualization, methodology, resources, visualization, supervision, project administration, writing—review and editing.

Funding
This work was supported by the Technology Innovation Program (RS-2023-00266009, Development of admixture and blended cement using unused inorganic resource) funded By the Ministry of Trade, Industry & Energy (MOTIE, Korea). This work was also supported by a grant from the Korea University.

Availability of data and materials
All data generated or analyzed during this study are included in this published article.

Declarations

Ethics approval and consent to participate
Not applicable.

Consent for publication
Not applicable.

Competing interests
The authors declare that they have no competing interests.

Received: 21 August 2024 Accepted: 14 May 2025
Published online: 01 August 2025

References

Acchar, W., & Dultra, E. J. V. (2013). Thermal analysis and X-ray diffraction of untreated coffee's husk ash reject and its potential use in ceramics. *Journal of Thermal Analysis and Calorimetry, 111*, 1331–1334. https://doi.org/10.1007/s10973-012-2478-0

Arulrajah, A., Kua, T. A., Phetchuay, C., Horpibulsuk, S., Mahghoolpilehrood, F., & Disfani, M. M. (2016). Spent Coffee Grounds-fly ash geopolymer used as an embankment structural fill material. *Journal of Materials in Civil Engineering, 28*, 04015197. https://doi.org/10.1061/(ASCE)MT.1943-5533.0001496

Arulrajah, A., Kua, T. A., Horpibulsuk, S., Mirzababaei, M., & Chinkulkijniwat, A. (2017a). Recycled glass as a supplementary filler material in spent coffee grounds geopolymers. *Construction and Building Materials, 151*, 18–27. https://doi.org/10.1016/j.conbuildmat.2017.06.050

Arulrajah, A., Kua, T. A., Suksiripattanapong, C., Horpibulsuk, S., & Shen, J. S. (2017b). Compressive strength and microstructural properties of spent coffee grounds bagasse ash based geopolymers with slag supplements. *Journal of Cleaner Production, 162*, 1491–1501. https://doi.org/10.1016/j.jclepro.2017.06.171

Arulrajah, A., Maghoolpilehrood, F., & Disfani, M. M. (2014). Spent coffee grounds as a non-structural embankment fill material: Engineering and environmental considerations. *Journal of Cleaner Production, 72*, 181–186. https://doi.org/10.1016/j.jclepro.2014.03.010

ASTM C192/C192M-19. (2019). Standard Practice for Making and Curing Concrete Test Specimens in the Laboratory, ASTM International, West Conshohocken, PA.

ASTM C150/C150M-21. (2021). Standard Specification for Portland Cement, ASTM International, West Conshohocken, PA.

ASTM C39/C39M-21. (2021). Standard Test Method for Compressive Strength of Cylindrical Concrete Specimens, ASTM International, West Conshohocken, PA.

ASTM D4284-12. (2012). Standard Test Method for Determining Pore Volume Distribution of Catalysts and Catalyst Carriers by Mercury Intrusion Porosimetry, ASTM International, West Conshohocken, PA.

Blinová, L., Sirotiak, M., Alica, B., & Maroš, S. (2017). Review: Utilization of waste from coffee production. *Research Papers Faculty of Materials Science and Technology Slovak University of Technology, 25*, 91–101. https://doi.org/10.1515/rput-2017-0011

Campos-Vega, R., Loarca-Piña, G., Vergara-Castañeda, H. A., & Oomah, B. D. (2015). Spent coffee grounds: A review on current research and future prospects. *Trends in Food Science & Technology, 45*, 24–36. https://doi.org/10.1016/j.tifs.2015.04.012

Cervera-Mata, A., Lara, L., Fernández-Arteaga, A., Rufián-Henares, J. Á., & Delgado, G. (2021). Washed hydrochar from spent coffee grounds: A second generation of coffee residues. *Evaluation as Organic Amendment. Waste Management, 120*, 322–329. https://doi.org/10.1016/j.wasman.2020.11.041

Cervera-Mata, A., Navarro-Alarcón, M., Rufián-Henares, J. Á., Pastoriza, S., Montilla-Gómez, J., & Delgado, G. (2020). Phytotoxicity and chelating capacity of spent coffee grounds: Two contrasting faces in its use as soil organic amendment. *Science of the Total Environment, 717*, 137247. https://doi.org/10.1016/j.scitotenv.2020.137247

Colantoni, A., Paris, E., Bianchini, L., Ferri, S., Marcantonio, V., Carnevale, M., Palma, A., Civitarese, V., & Gallucci, F. (2021). Spent coffee ground characterization, pelletization test and emissions assessment in the combustion process. *Scientific Reports, 11*, 5119. https://doi.org/10.1038/s41598-021-84772-y

Franklin, G., & Dias, A. C. P. (2011). Chlorogenic acid participates in the regulation of shoot, root and root hair development in Hypericum perforatum. *Plant Physiology and Biochemistry, 49*, 835–842. https://doi.org/10.1016/j.plaphy.2011.05.009

Janissen, B., & Huynh, T. (2018). Chemical composition and value-adding application of coffee industry by-products: A review. *Resources, Conservation and Recycling, 128*, 110–117. https://doi.org/10.1016/j.resconrec.2017.10.001

Kang, S. B., Oh, H. Y., Kim, J. J., & Choi, K. S. (2017). Characteristics of spent coffee ground as a fuel and combustion test in a small boiler (6.5 kW). *Renewable Energy, 113*, 1208–1214. https://doi.org/10.1016/j.renene.2017.06.092

Kim, M.-J., Choi, S. W., Kim, H., Mun, S., & Lee, K. B. (2020). Simple synthesis of spent coffee ground-based microporous carbons using K_2CO_3 as an activation agent and their application to CO_2 capture. *Chemical Engineering Journal, 397*, 125404. https://doi.org/10.1016/j.cej.2020.125404

Kua, T. A., Arulrajah, A., Horpibulsuk, S., Du, Y. J., & Shen, S. L. (2016). Strength assessment of spent coffee grounds-geopolymer cement utilizing slag and fly ash precursors. *Construction and Building Materials, 115*, 565–575. https://doi.org/10.1016/j.conbuildmat.2016.04.021

Kua, T. A., Arulrajah, A., Mohammadinia, A., Horpibulsuk, S., & Mirzababaei, M. (2017). Stiffness and deformation properties of spent coffee grounds based geopolymers. *Construction and Building Materials, 138*, 79–87. https://doi.org/10.1016/j.conbuildmat.2017.01.082

Kua, T. A., Imteaz, M. A., Arulrajah, A., & Horpibulsuk, S. (2019). Environmental and economic viability of alkali activated material (AAM) comprising slag, fly ash and spent coffee ground. *International Journal of Sustainable Engineering, 12*, 223–232. https://doi.org/10.1080/19397038.2018.1492043

Le, T. T., Park, S. S., Lee, J. C., & Lee, D. E. (2021). Strength characteristics of spent coffee grounds and oyster shells cemented with GGBS-based alkaline-activated materials. *Construction and Building Materials, 267*, 120986. https://doi.org/10.1016/j.conbuildmat.2020.120986

Lee, K.-T., Tasi, J.-Y., Hoang, A. T., Chen, W.-H., Gunarathne, D. S., Tran, K.-Q., Selvarajoo, A., & Goodarzi, V. (2022). Energy-saving drying strategy of spent coffee grounds for co-firing fuel by adding biochar for carbon

sequestration to approach net zero. *Fuel, 326*, 124984. https://doi.org/10.1016/j.fuel.2022.124984
Limousy, L., Jeguirim, M., Dutournié, P., Kraiem, N., Lajili, M., & Said, R. (2013). Gaseous products and particulate matter emissions of biomass residential boiler fired with spent coffee grounds pellets. *Fuel, 107*, 323–329. https://doi.org/10.1016/j.fuel.2012.10.019
Liu, K., & Price, G. W. (2011). Evaluation of three composing system for the management of spent coffee grounds. *Bioresource Technology, 102*, 7966–7974. https://doi.org/10.1016/j.biortech.2011.05.073
Makar, J. M., & Chan, G. W. (2009). Growth of cement hydration products on single-walled carbon nanotubes. *Journal of the American Ceramic Society, 92*, 1303–1310. https://doi.org/10.1111/j.1551-2916.2009.03055.x
Metha, P. K., & Monteiro, P. J. M. (2014). *Concrete: Microstructure, properties and materials* (4th ed.). McGraw-Hill Education.
Murthy, P. S., & Madhava Naidu, M. (2012). Sustainable management of coffee industry by-products and value addition—A review. *Resources, Conservation and Recycling, 66*, 45–58. https://doi.org/10.1016/j.resconrec.2012.06.005
Najdanovic-Visak, V., Lee, F. Y. L., Tavares, M. T., & Armstrong, A. (2017). Kinetics of extraction and in situ transesterification of oils from spent coffee grounds. *Journal of Environmental Chemical Engineering, 5*, 2611–2616. https://doi.org/10.1016/j.jece.2017.04.041
Namane, A., Mekarzia, A., Benrachedi, K., Belhaneche-Bensemra, N., & Hellal, A. (2005). Determination of the adsorption capacity of activated carbon made from coffee grounds by chemical activation with $ZnCl_2$ and H_3PO_4. *Journal of Hazardous Materials, 119*, 189–194. https://doi.org/10.1016/j.jhazmat.2004.12.006
NT BUILD 492. (1999). Concrete, Mortar and Cement-Based Repair Materials: Chloride Migration Coefficient from Non-Steady-State Migration Experiments. Nordtest, Finland.
Pagalan, E., Sebron, M., Gomez, S., Salva, S. J., Ampusta, R., Macarayo, A. J., Joyno, C., Ido, A., & Arazo, R. (2020). Activated carbon from spent coffee grounds as an adsorbent for treatment of water contaminated by aniline yellow. *Industrial Crops and Products, 145*, 111953. https://doi.org/10.1016/j.indcrop.2019.111953
Park, S. Y., Kim, S. J., Oh, K. C., Cho, L. H., Kim, M. J., Jeong, I. S., Lee, C. G., & Kim, D. H. (2020). Investigation of agro-byproduct pellet properties and improvement in pellet quality through mixing. *Energy, 190*, 116380. https://doi.org/10.1016/j.energy.2019.116380
Péra, J., Husson, S., & Guilhot, B. (1999). Influence of finely ground limestone on cement hydration. *Cement and Concrete Composites, 21*(2), 99–105. https://doi.org/10.1016/S0958-9465(98)00020-1
Qiang, W., Mengxiao, S., & Dengquan, W. (2016). Contributions of fly ash and ground granulated blast-furnace slag to the early hydration heat of composite binder at different curing temperatures. *Advances in Cement Research, 28*, 320–327. https://doi.org/10.1680/jadcr.15.00077
Roychand, R., Kilmartin-Lynch, S., Saberian, M., Li, J., & Li, C. Q. (2025). Translating lab success to the field: Evaluating coffee biochar-enhanced concrete in real-world construction. *Case Studies in Construction Materials, 22*, Article e04233. https://doi.org/10.1016/j.cscm.2025.e04233
Roychand, R., Kilmartin-Lynch, S., Saberian, M., Li, J., Zhang, G., & Li, C. Q. (2023). Transforming spent coffee grounds into a valuable resource for the enhancement of concrete strength. *Journal of Cleaner Production, 419*, 138205. https://doi.org/10.1016/j.jclepro.2023.138205
Saberian, M., Li, J., Donnoli, A., Bonderenko, E., Oliva, P., Gill, B., Lockery, S., & Siddique, R. (2021). Recycling of spent coffee grounds in construction materials: A review. *Journal of Cleaner Production, 289*, 125837. https://doi.org/10.1016/j.jclepro.2021.125837
Santos, C., Fonseca, J., Aires, A., Coutinho, J., & Trindade, H. (2017). Effect of different rates of spent coffee grounds (SCG) on composting process, gaseous emissions and quality of end-product. *Waste Management, 59*, 37–47. https://doi.org/10.1016/j.wasman.2016.10.020
Setter, C., Borges, F. A., Cardoso, C. R., Mendes, R. F., & Oliveira, T. J. P. (2020). Energy quality of pellets produced from coffee residue: Characterization of the products obtained via slow pyrolysis. *Industrial Crops and Products, 154*, 112731. https://doi.org/10.1016/j.indcrop.2020.112731
Shao, J., Chen, Z., Luo, S., Liu, S., Sun, X., Wen, H., & Su, L. (2024). Evaluation on the effect of modified treatment of spent coffee grounds on the concrete performance. *Journal of Building Engineering, 97*, 110910. https://doi.org/10.1016/j.jobe.2024.110910
Statista.com. (2022). Coffee consumption worldwide from 2012/13 to 2020/21 (in million 60kg bags). https://www.statista.com/statistics/292595/global-coffee-consumption/. Accessed 20 June 2022
Suksiripattanapong, C., Kua, A. T., Arulrajah, A., Maghool, F., & Horpibulsuk, S. (2017). Strength and microstructure properties of spent coffee grounds stabilized with rice husk ash and slag geopolymers. *Construction and Building Materials, 146*, 312–320. https://doi.org/10.1016/j.conbuildmat.2017.04.103

Publisher's Note

Yoonsuk Choi Yoonsuk Choi is a Senior Research Engineer at the Smart Construction Materials Center of Korea Conformity Laboratories. His research interests include supplementary cementitious materials, carbonation, chloride ion penetration, and sustainable concrete technologies. He focuses on the durability and eco-efficiency of cementitious materials for resilient infrastructure. Dr. Choi actively participates in national R&D projects and international collaborations in the field of sustainable construction.

Byoungsun Park Byoungsun Park is an Associate Professor in the Department of Environmental Systems Engineering at Korea University. His research interests include the durability of concrete, nondestructive evaluation of concrete, supplementary cementitious materials, and low-carbon construction materials.